

Graph Out-of-Distribution Generalization via Causal Intervention

Qitian Wu
Shanghai Jiao Tong University
Shanghai, China
echo740@sjtu.edu.cn

Fan Nie
Shanghai Jiao Tong University
Shanghai, China
youluo2001@sjtu.edu.cn

Chenxiao Yang
Shanghai Jiao Tong University
Shanghai, China
chr26195@sjtu.edu.cn

Tianyi Bao
Shanghai Jiao Tong University
Shanghai, China
btyll05@sjtu.edu.cn

Junchi Yan*
Shanghai Jiao Tong University
Shanghai, China
yanjunchi@sjtu.edu.cn

ABSTRACT

Out-of-distribution (OOD) generalization has gained increasing attentions for learning on graphs, as graph neural networks (GNNs) often exhibit performance degradation with distribution shifts. The challenge is that distribution shifts on graphs involve intricate interconnections between nodes, and the environment labels are often absent in data. In this paper, we adopt a bottom-up data-generative perspective and reveal a key observation through causal analysis: the crux of GNNs' failure in OOD generalization lies in the latent confounding bias from the environment. The latter misguides the model to leverage environment-sensitive correlations between ego-graph features and target nodes' labels, resulting in undesirable generalization on new unseen nodes. Built upon this analysis, we introduce a conceptually simple yet principled approach for training robust GNNs under node-level distribution shifts, without prior knowledge of environment labels. Our method resorts to a new learning objective derived from causal inference that coordinates an environment estimator and a mixture-of-expert GNN predictor. The new approach can counteract the confounding bias in training data and facilitate learning generalizable predictive relations. Extensive experiment demonstrates that our model can effectively enhance generalization with various types of distribution shifts and yield up to 27.4% accuracy improvement over state-of-the-arts on graph OOD generalization benchmarks. Source codes are available at <https://github.com/fannie1208/CaNet>.

CCS CONCEPTS

• **Computing methodologies** → **Machine learning algorithms; Machine learning approaches; Causal reasoning and diagnostics; Probabilistic reasoning.**

Correspondence author. The work was partly supported by NSFC (92370201, 62222607) and SJTU Trans-med Awards Research (STAR) (20210106).

Permission to make digital or hard copies of all or part of this work for personal or classroom use is granted without fee provided that copies are not made or distributed for profit or commercial advantage and that copies bear this notice and the full citation on the first page. Copyrights for components of this work owned by others than the author(s) must be honored. Abstracting with credit is permitted. To copy otherwise, or republish, to post on servers or to redistribute to lists, requires prior specific permission and/or a fee. Request permissions from permissions@acm.org.

WWW '24, May 13–17, 2024, Singapore, Singapore

© 2024 Copyright held by the owner/author(s). Publication rights licensed to ACM.
ACM ISBN 979-8-4007-0171-9/24/05...\$15.00
<https://doi.org/10.1145/3589334.3645604>

KEYWORDS

Graph Representation Learning, Graph Neural Networks, Distribution Shifts, Out-of-Distribution Generalization, Causal Inference

ACM Reference Format:

Qitian Wu, Fan Nie, Chenxiao Yang, Tianyi Bao, and Junchi Yan. 2024. Graph Out-of-Distribution Generalization via Causal Intervention. In *Proceedings of the ACM Web Conference 2024 (WWW '24)*, May 13–17, 2024, Singapore, Singapore. ACM, New York, NY, USA, 11 pages. <https://doi.org/10.1145/3589334.3645604>

1 INTRODUCTION

Graph neural networks (GNNs) [10, 12, 12, 14, 29, 35] have emerged as a de facto class of encoder backbones for modeling interdependent data and efficiently computing node representations that can be readily adapted to diverse graph-based applications, including social network analysis [33], recommender systems [38], clinical healthcare [44], traffic control [11], anomaly detection [46], etc.

Despite solid advances in the expressivity and representational power of GNNs, most of existing models focus on improving the accuracy on in-distribution data, i.e., the testing nodes generated from an identical distribution as the training ones. However, recent evidence [39, 43, 45, 47] suggests that GNNs can perform unsatisfactorily on out-of-distribution (OOD) data where the data-generating distributions exhibit differences from training observations.

We illustrate such an issue through a typical example for node property prediction with GNNs, as shown in Fig. 1. Let us consider a social network where the nodes correspond to users and the goal is to predict whether a user likes playing basketball. In general, if a user's friends love sports, then the conditional probability for the user liking basketball would be high, which can be treated as a stable (or interchangeably, *environment-insensitive*) relation from the *ego-graph feature* (the GNN model actually processes as input of each node) to the *label* of the target node. Yet, there also exists positive correlation between "a user's friends are young" and "the user likes basketball" on condition that the social network is formed in a university where the marginal probability for "a user's friends are young" and "a user likes playing basketball" are both high. The relation from such an ego-graph feature to the label is unstable (or interchangeably, *environment-sensitive*), since this correlation does not hold elsewhere like LinkedIn where the marginal distributions for user's ages and hobbies have considerable diversity. The prediction relying on the latter unstable relation would fail once the environment changes from universities to LinkedIn, which causes

to represent the data distribution (p_{tr}/p_{te} is used for specifying training/testing data) while p_θ denotes the predictive distribution induced by the model with parameterization θ . Besides, q and q_ϕ denote other distributions, typically the variational distributions.

Predictive Tasks on Graphs. Assume a graph $\mathcal{G} = (\mathcal{V}, \mathcal{E})$ with N nodes, where \mathcal{V} and \mathcal{E} denote the node set and edge set, respectively. Besides, $\mathbf{X} = [\mathbf{x}_v]_{v \in \mathcal{V}} \in \mathbb{R}^{N \times D}$ denotes the node feature matrix, where D is the input feature dimension, and $\mathbf{A} = [a_{vu}]_{v,u \in \mathcal{V}} \in \{0, 1\}^{N \times N}$ denotes the adjacency matrix. If there exists an edge between node u and v , then $a_{uv} = 1$, and otherwise 0. Each node corresponds to a label, denoted by a one-hot vector $\mathbf{y}_v \in \{0, 1\}^C$ where C is the number of classes. The predictive tasks on graphs can be defined as: given labels $\{\mathbf{y}_v\}_{v \in \mathcal{V}_{tr}}$ for training nodes \mathcal{V}_{tr} , one aims to predict labels $\{\mathbf{y}_v\}_{v \in \mathcal{V}_{te}}$ for testing nodes $\mathcal{V}_{te} = \mathcal{V} \setminus \mathcal{V}_{tr}$ with node features \mathbf{X} and graph adjacency \mathbf{A} .

From a data-generating perspective, the input graph \mathcal{G} can be seen as a collection of (overlapping) pieces of ego-networks [22, 39]. For node v , its L -hop ego-graph is denoted as $\mathcal{G}_v^{(L)} = (\mathbf{X}_v^{(L)}, \mathbf{A}_v^{(L)})$ where $\mathbf{X}_v^{(L)}$ and $\mathbf{A}_v^{(L)}$ are the node feature matrix and the adjacency matrix induced by nodes in v 's L -hop neighborhood. To keep notations clean, we omit the superscript and use \mathcal{G}_v to represent the ego-graph of v unless otherwise specified for emphasizing the order. Furthermore, we define G as a random variable of ego-graphs \mathcal{G}_v 's and Y as a random variable for node labels \mathbf{y}_v 's.

Distribution Shifts on Graphs. The distribution shifts induce that $p_{tr}(G, Y) \neq p_{te}(G, Y)$, i.e. the data distributions that generate the ego-graphs and labels of training and testing nodes are different. A crucial concept in OOD generalization is the *environment*¹ that serves as the direct cause for the data-generating distribution [39]. In node property prediction, the *environment* can be a general reflection for where or when the nodes in a graph are generated. For example, as shown by the social network example in Section 1, the environment is where the graph is collected ("university" or "LinkedIn"). In protein networks [51], the environment can be the species that the protein belongs to. In citation networks [13], the environment can be when the paper is published (e.g., "before 2010" or "from 2010 to 2015"). The specific physical meanings for environments depend on particular datasets. Without loss of generality, define E as the random variable of environments and e as its realization, and the data-generating distribution can be characterized by $P(G, Y|E) = P(G|E)P(Y|G, E)$, i.e., E impacts the generation process of G and Y . Fig. 1(c) illustrates the dependence of three random variables through a causal diagram which highlights that the environment E is the common cause for G and Y .

4 PROPOSED MODEL

We next present our analysis and proposed method. In Section 4.1, we first analyze the generalization behaviors of common GNNs in node property prediction under distribution shifts and reveal what causes the deficiency of GNNs w.r.t. out-of-distribution data. Based on the analysis, in Section 4.2 and 4.3, we introduce the formulation and instantiations for our proposed model, respectively.

¹In OOD generalization literature [5, 9, 26], *environment* and *domain* are interchangeably used and refer to an indicator of which distribution a sample is generated from.

4.1 Causal Analysis for Graph Neural Networks

To understand the generalization behaviors of GNNs, we present a proof-of-concept causal analysis on the dependence among variables of interest regarding node property prediction. The results attribute the failure of GNN models for out-of-distribution (OOD) generalization to the confounding bias of unobserved environments.

The Confounding Bias of Latent Environments. Common GNN models take a graph \mathcal{G} as input, iteratively update node representations through aggregating neighbored nodes' features and output the estimated label for each node. Specifically, assume $\mathbf{z}_v^{(l)}$ as the representation of node v at the l -th layer and the updating rule of common GNNs can be written as

$$\mathbf{z}_v^{(l+1)} = \sigma \left(\text{Conv}^{(l)} \left(\{\mathbf{z}_u^{(l)} \mid u \in \mathcal{N}_v \cup \{v\}\} \right) \right), \quad (1)$$

where \mathcal{N}_v is the set of nodes connected with v in the graph and $\text{Conv}^{(l)}$ is a graph convolution operator over node representations. For example, in vanilla GCN [14], $\text{Conv}^{(l)}$ is instantiated as a parameterized linear transformation of node representations and a normalized aggregation. Also, the initial node embeddings are often computed by the node features $\mathbf{z}_v^{(1)} = \phi_{in}(\mathbf{x}_v)$ and the predicted labels are given by the last-layer embeddings $\hat{\mathbf{y}}_v = \phi_{out}(\mathbf{z}_v^{(L+1)})$ if using L layers of propagation. Here ϕ_{in} and ϕ_{out} can be shallow neural networks. Notice that, for each node v , what the GNN model actually processes as input for prediction is its ego-graph \mathcal{G}_v (in particular, for an L -layer GNN, \mathcal{G}_v consists of all the L -hop neighbored nodes centered at v). Therefore, the prediction for node v can be denoted by $\hat{\mathbf{y}}_v = f_\theta(\mathcal{G}_v)$ where f_θ denotes the GNN model with trainable parameter set θ . We define \hat{Y} as a random variable for predicted node labels $\hat{\mathbf{y}}_v$'s and $p_\theta(\hat{Y}|G)$ denotes the predictive distribution induced by the model f_θ .

The common practice is to adopt maximum likelihood estimation (MLE) as the training objective which maximizes the likelihood $p_\theta(\hat{Y}|G)$. For node property prediction, the negative log-likelihood that is minimized as training objective is the cross-entropy loss:

$$\theta^* = \arg \min_{\theta} -\frac{1}{|\mathcal{V}_{tr}|} \sum_{v \in \mathcal{V}_{tr}} \mathbf{y}_v^\top \log f_\theta(\mathcal{G}_v). \quad (2)$$

Based on the above illustration of the GNN's modeling and learning on graphs, the dependence among the (input) ego-graph G , the predicted label \hat{Y} and the latent environment E can be characterized by another causal diagram as shown in Fig. 2(a). We next illustrate the rationales behind each dependence edge shown in Fig. 2(a).

- $G \rightarrow \hat{Y}$. The dependence is given by the feed-forward computation of GNN model $\hat{\mathbf{y}}_v = f_\theta(\mathcal{G}_v)$, i.e., the model predictive distribution $p_\theta(\hat{Y}|G)$. The relation between G and Y becomes deterministic if given fixed model parameter θ .
- $E \rightarrow G$. This dependence is given by $p(G|E)$ in data generation.
- $E \rightarrow \hat{Y}$. This relation is embodied through the learning process. Since E affects the distribution for observed data via $p(G, Y|E) = p(G|E)p(Y|G, E)$, if we denote by $p_{tr}(E)$ the distribution for (unobserved) training environments, the learning algorithm yields

$$\theta^* = \arg \min_{\theta} \mathbb{E}_{e \sim p_{tr}(E), (\mathcal{G}_v, \mathbf{y}_v) \sim p(G, Y|E=e)} [-\mathbf{y}_v^\top \log f_\theta(\mathcal{G}_v)]. \quad (3)$$

This suggests that the well-trained model parameter θ^* is dependent on the distribution of E , leading to the dependence of \hat{Y} on E . Such a causal relation can also be interpreted intuitively with two facts:

1) E affects the generation of data used for training the GNN model, and 2) \hat{Y} is the output of the trained model.

Interpretations for Harmful Effects. From Fig. 2(a) and the above illumination, we can see that if we optimize the likelihood $p_\theta(\hat{Y}|G)$, the confounding effect of E on G and \hat{Y} will mislead the GNN model to capture the shortcut predictive relation between the ego-graph \mathcal{G}_v and the label y_v , i.e., the existing correlation that is induced by certain e 's in training data (e.g., " \mathcal{G}_v : a user's friends are young" and " y_v : the user likes playing basketball" are both with high probability due to the unobserved environment e "university" in social networks). Therefore, the training process would incline to purely increase the training accuracy by exploiting such easy-to-capture yet unreliable correlation (e.g., the predictive relation from " \mathcal{G}_v : a user's friends are young" to " y_v : the user likes playing basketball") in observational data. The issue, however, is that this kind of correlation is non-stable and sensitive to distribution shifts: for testing data that has distinct environment context, i.e., $P_{te}(E) \neq P_{tr}(E)$ (e.g., testing users are from another environment "LinkedIn"), the above-mentioned correlation does not necessarily hold. The model that mistakenly over-fits the environment-sensitive relations in training data would suffer from failures or undesired prediction on out-of-distribution data in testing stage.

Implications for Potential Solutions. The analysis enlightens one potential solution for improving the OOD generalization ability of GNNs in node property prediction: one can guide the model to uncover the stable predictive relations behind data, particularly the ones insensitive to environment variation (e.g., the relation from " \mathcal{G}_v : a user's friends love sports" to " y_v : the user likes playing basketball"). Formally speaking, we can train the model by optimizing $p_\theta(\hat{Y}|do(G))$, where in causal literature the do -operation means removing the dependence from other variables on the target, to cancel out the effect of E on G such that the unstable correlation between \mathcal{G}_v and y_v will no longer be captured by the model. Compared with $p_\theta(\hat{Y}|G)$ where the condition is on a given observation \mathcal{G}_v of G , the do -operation in $p_\theta(\hat{Y}|do(G))$ enforces the condition that intervenes the value of G as \mathcal{G}_v and removes the effects from other variables on G (i.e., E in our case), as conceptually shown by Fig. 2(b). We next discuss how to put this general idea into practice.

4.2 Model Formulation: A Causal Treatment

An ideal way for exactly computing $p_\theta(\hat{Y}|do(G))$ is to physically intervene G , e.g., by randomized controlled trial (RCT) [25] where data is recollected from a prohibitively large quantity of random samples. The randomized experiments gather new data that removes the bias from the environment by enumerating any possible environment context in a physical scene, based on which the model can learn stable relations from G to Y and generalize well to new distributions. Nevertheless, this can be intractable due to limited resources in practice. We thereby resort to a learning approach based on observational data (i.e., \mathcal{G}_v 's and y_v 's).

First, we harness the backdoor adjustment [25] that gives rise to (see derivation in Appendix A.1)

$$p_\theta(\hat{Y}|do(G)) = \mathbb{E}_{p_0(E)} [p_\theta(\hat{Y}|G, E)], \quad (4)$$

where p_0 is the prior distribution of environments that reflects how plausible the environment context could happen without any

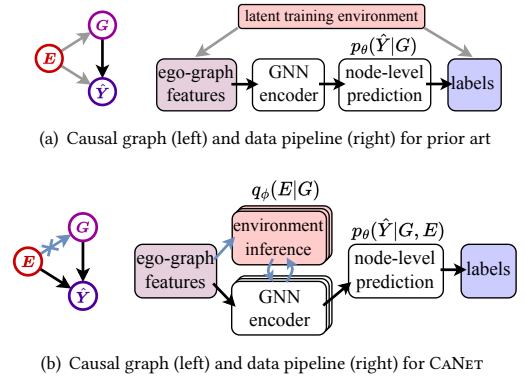


Figure 2: Structural Causal Models and data pipelines for (a) standard GNNs' learning process and (b) our proposed approach CANET's. The training of common GNNs is affected by the latent confounder E that misguides the model to rely on environment-insensitive correlation between G and Y and leads to unsatisfactory OOD generalization. In contrast, our approach resorts to a new learning objective that essentially cuts off the dependence between E and G .

information of observed data. Though we have known that the latent environment plays an important role in data generation and impact the generalizability of GNNs, the actual meaning or form of environments is often unknown. This leads to the difficulty of instantiating $p_\theta(\hat{Y}|G, E)$ to particular forms involving the effect of the environments on the prediction. Even for cases where the environment information could be partially reflected by certain node features (e.g., publication years of papers in citation networks or species groups of proteins in PPI networks), we empirically found that the environment labels may not be informative enough for guiding GNNs to learn stable relations with distribution shifts. To effectively handle the confounding effects of unobserved environments, we next introduce an approximation method by inferring the latent environments in a data-driven manner.

Approximated Intervention with Environment Inference. Our basic idea is to generate pseudo environment labels as latent variables (agnostic of specific actual environments) that are regularized to be independent of the ego-graph features and guide the model to capture stable relations between G and Y . To implement this idea, we consider collaborative learning of two models: i) an environment estimator $q_\phi(E|G)$ with parameterization ϕ that takes the ego-graph features \mathcal{G}_v as input to infer the pseudo environment e_v for node v ; ii) a GNN predictor $p_\theta(\hat{Y}|G, E)$ whose prediction is based on input ego-graph \mathcal{G}_v and the inferred pseudo environment e_v . The learning objective can be derived from a variational lower bound of Eqn. 4 (see derivation in Appendix A.2):

$$\begin{aligned} & \log p_\theta(\hat{Y}|do(G)) \\ & \geq \underbrace{\mathbb{E}_{q_\phi(E|G)} [\log p_\theta(\hat{Y}|G, E)]}_{-\mathcal{L}_{sup}} - \underbrace{KL(q_\phi(E|G) \| p_0(E))}_{-\mathcal{L}_{reg}}. \quad (5) \end{aligned}$$

The first term can optimize the predictive power of the GNN and the second term regularizes that the pseudo environments should be independent of ego-graphs. The maximization of Eqn. 5 contributes to lifting the variational lower bound of $p_\theta(\hat{Y}|do(G))$ that

facilitates the GNN model $p_\theta(\hat{Y}|G, E)$ trained with inferred pseudo environments to capture the stable correlation between ego-graphs and labels. The learning objective of Eqn. 5 approximately achieves the ideal goal (of causal intervention) such that the model’s prediction would be guided to be primarily based on the environment-insensitive patterns in G and robust to distribution shifts.

4.3 Model Instantiations

Notice again that we do not require environment labels in data or any prior knowledge of the physical meaning of unobserved environments, and neither require that the pseudo environments should reflect the actual contextual information. Therefore, we assume the pseudo environments as latent variables represented by numerical vectors for each node v . Nevertheless, we expect the representation of the pseudo environments to be informative enough, on top of which the model can learn useful patterns from observed data to benefit learning stable relations for better generalization. As mentioned in Section 1, one observation is that the distribution shifts on graphs often involve inter-connection of nodes, i.e., the structural features of ego-graphs can be informative and contain the desired stable patterns. Therefore, for better capacity, we generalize the notion of pseudo environments to a series of vector representations pertaining to each layer of the GNN model, as illustrated in Fig. 3 with details described below.

Pseudo Environment Estimator $q_\phi(E|G)$. We assume $\mathbf{e}_v^{(l)} \in \mathbb{R}^K$ as the inferred pseudo environment for node v at the l -th layer of feature aggregation. Here $\mathbf{e}_v^{(l)}$ is a K -dimensional numerical vector and can be modeled by a categorical distribution $\mathcal{M}(\boldsymbol{\pi}_v^{(l)})$ where $\mathbf{e}_v^{(l)}$ is sampled. We model the probabilities $\boldsymbol{\pi}_v^{(l)}$ conditioned on the node representations $\{\mathbf{z}_v^{(l)}\}$ at the current layer:

$$\boldsymbol{\pi}_v^{(l)} = \text{Softmax}(\mathbf{W}_S^{(l)} \mathbf{z}_v^{(l)}), \quad (6)$$

where $\mathbf{W}_S^{(l)} \in \mathbb{R}^{H \times K}$ is a trainable weight matrix and H is the hidden dimension of $\mathbf{z}_v^{(l)}$. Since sampling $\mathbf{e}_v^{(l)}$ from $\mathcal{M}(\boldsymbol{\pi}_v^{(l)})$ would result in non-differentiability, to enable back-propagation for training, we adopt the Gumbel-Softmax trick [23] which specifically gives (for $k = 1, \dots, K$)

$$e_{vk}^{(l)} = \frac{\exp\left(\left(\pi_{vk}^{(l)} + g_k\right)/\tau\right)}{\sum_k \exp\left(\left(\pi_{vk}^{(l)} + g_k\right)/\tau\right)}, \quad g_k \sim \text{Gumbel}(0, 1), \quad (7)$$

where g_k is a noise sampled from Gumbel distribution and τ controls the closeness of the result to discrete samples. Since in our case we do not require that the pseudo environment should be a categorical variable, we can still use moderate value for τ (e.g., $\tau = 1$ which we found works smoothly in practice).

Mixture-of-Expert GNN Predictor $p_\theta(\hat{Y}|G, E)$. The GNN predictor aims to encode input ego-graph \mathcal{G}_v conditioned on the inferred pseudo environment e_v given by $q_\phi(E|G)$. To accommodate the layer-specific environment inference, we consider layer-wise updating controlled by K mixture-of-expert (MoE) propagation units, instantiated by two models. The first model implements a

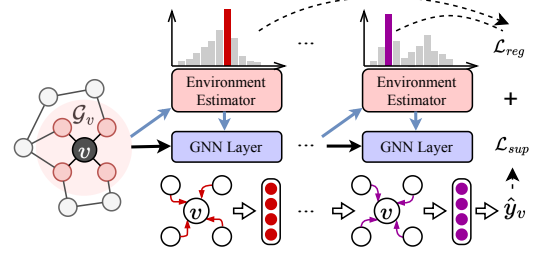


Figure 3: Illustration for the proposed model CANET whose layer-wise computation entails a layer-specific environment estimator and a special feature propagation layer conditioned on the inferred pseudo environment.

GCN-like MoE architecture with layer-wise updating rule:

$$\mathbf{z}_u^{(l+1)} = \sigma \left(\sum_{k=1}^K e_{u,k}^{(l)} \sum_{v, a_{uv}=1} \frac{1}{\sqrt{d_u d_v}} \mathbf{W}_D^{(l,k)} \mathbf{z}_v^{(l)} + \mathbf{W}_S^{(l,k)} \mathbf{z}_u^{(l)} \right), \quad (8)$$

where d_u denotes the degree of node u , $\mathbf{W}_D^{(l,k)} \in \mathbb{R}^{H \times H}$ and $\mathbf{W}_S^{(l,k)}$ are trainable weight matrices for the k -th branch at the l -th layer, and σ denotes activation function (e.g., ReLU). We call this model implementation CANET-GCN that can be seen as a generalized implementation of Graph Convolution Networks [14], where $\mathbf{e}_u^{(l)}$ dynamically selects convolution filters among K candidates in each layer for propagation. In the second model, we further harness an attention network for each branch to model the adaptive pairwise influence between connected nodes:

$$\mathbf{z}_u^{(l+1)} = \sigma \left(\sum_{k=1}^K e_{u,k}^{(l)} \sum_{v, a_{uv}=1} w_{uv}^{(l,k)} \mathbf{W}_D^{(l,k)} \mathbf{z}_v^{(l)} + \mathbf{W}_S^{(l,k)} \mathbf{z}_u^{(l)} \right), \quad (9)$$

$$w_{uv}^{(l,k)} = \frac{\text{LeakyReLU}(\mathbf{b}^{(l,k)})^\top [\mathbf{W}_A^{(l,k)} \mathbf{z}_u^{(l)} \parallel \mathbf{W}_A^{(l,k)} \mathbf{z}_v^{(l)}]}{\sum_{w=1}^N \text{LeakyReLU}(\mathbf{b}^{(l,k)})^\top [\mathbf{W}_A^{(l,k)} \mathbf{z}_u^{(l)} \parallel \mathbf{W}_A^{(l,k)} \mathbf{z}_w^{(l)}]}, \quad (10)$$

where $\mathbf{W}_A^{(l,k)} \in \mathbb{R}^{H \times H}$ and $\mathbf{b}^{(l,k)} \in \mathbb{R}^{2H}$ are trainable parameters. The model which we call CANET-GAT can be seen as a generalized version of Graph Attention Networks [35] with K attention networks in each layer selected by $\mathbf{e}_u^{(l)}$ for attentive propagation.

With L -layer propagation, the model (with instantiation (8) or (9)) outputs $\mathbf{z}_u^{(L+1)}$ that is further transformed by a fully-connected layer into node-wise prediction \hat{y}_v . The above models extend the notion of environments for each node v to a series of layer-specific vectors $\{\mathbf{e}_v^{(l)}\}_{l=1}^L$ that control the propagation network in each GNN layer. Such a design allows sufficient interactions between two modules: 1) the GNN’s message passing helps to combine neighbored information in \mathcal{G}_v conditioned on layer-specific environment inference (as given by (6)); 2) the inferred pseudo environments endow the GNN predictor with adaptive feature propagation w.r.t. different contexts (as defined by (8) and (9)). This guides each layer of the GNN predictor to extract stable relations from ego-graph features, particularly the complex structural patterns that are informative for prediction and insensitive to distribution shifts.

Optimization and Algorithm. For model training, we adopt gradient-based optimization for q_ϕ and p_θ with the objective (5). We assume $p_0(E)$ for pseudo environments as a trivial uniform

distribution (with equal probabilities for K possible choices) and the loss function induced by (5) can be written as

$$\frac{1}{|\mathcal{V}_{tr}|} \sum_{v \in \mathcal{V}_{tr}} \left[-\mathbf{y}_v^\top \log \hat{\mathbf{y}}_v + \frac{\lambda}{L} \sum_{l=1}^L \sum_{k=1}^K \left[e_{vk}^{(l)} \log \pi_{vk}^{(l)} + e_{vk}^{(l)} \log K \right] \right], \quad (11)$$

where λ is a hyper-parameter weight. Alg. 1 in the appendix presents the model’s feed-forward and training. The complexity of our model is $O(LK|\mathcal{E}|)$, where $|\mathcal{E}|$ denotes the number of edges in the graph.

5 EXPERIMENTS

We apply our model to various datasets to evaluate its generalization capability. Overall, we aim to answer the questions:

- (R1) How does CANET perform compared to state-of-the-art models for handling distribution shifts on graphs?
- (R2) Are the proposed components of CANET effective for OOD generalization?
- (R3) What is the sensitivity of CANET w.r.t. the number of MoE branches (K) and the Gumbel-Softmax temperature (τ)?
- (R4) Do different propagation branches learn different patterns?

5.1 Experiment Setup

Datasets. We adopt six node property prediction datasets of different sizes and properties, including Cora, Citeseer, Pubmed, Twitch, Arxiv and Elliptic. Following [39], we consider different ways to construct an in-distribution (ID) portion and an out-of-distribution (OOD) portion for each dataset. For Cora, Citeseer and Pubmed [30], we keep the original node labels and synthetically create spurious node features to introduce distribution shifts between ID and OOD data. For Arxiv [13], we use publication years for data splits: papers published within 2005-2014 as ID data and after 2014 as OOD data. For Twitch [27], we consider subgraph-level data splits: nodes in the subgraph DE, PT and RU as ID data, and nodes in ES, FR and EN as OOD data. For Elliptic [24], we use the first five graph snapshots as ID data and the remaining as OOD data. We summarize the dataset information in Table 2, with detailed descriptions and preprocessing presented in Appendix B.

Evaluation Protocol. For each dataset, the nodes of ID data are further randomly split into training/validation/testing with the ratio 50%/25%/25%. We use the training data for model training and the performance on validation data for model selection and early stopping. We test the model with the performance on both the testing data within the ID portion and the OOD data, respectively, where the latter quantifying the OOD generalization capabilities is our major focus. We follow the common practice, and use Accuracy as the metric for Cora, Citeseer, Pubmed and Arxiv, ROC-AUC for Twitch, and macro F1 score for Elliptic. We run the experiment for each case with five trails using different initializations and report the means and standard deviations for the metric.

Competitors. We basically compare with empirical risk minimization (ERM) that trains the model with standard supervised loss. We adopt GCN and GAT as the backbone to compare with CANET-GCN and CANET-GAT, respectively. Besides, we consider two sets of competitors that are agnostic to encoder backbones. The first line of models are designed for OOD generalization in general settings (where the instances, e.g., images, are assumed

to be independent), including IRM [1], DeepCoral [32], DANN [8], GroupDRO [28] and Mixup [48]. Another line of works focus on learning with distribution shifts and out-of-distribution generalization on graphs, including the state-of-the-art models SR-GNN [50] and EERM [39]. For all the competitors, we use GCN and GAT as their encoder backbones, respectively. Details for implementation and competitors are deferred to Appendix C.

5.2 Comparative Results (R1)

Distribution Shifts on Synthetic Data. We report the testing accuracy on Cora, Citeseer and Pubmed in Table 1. We found that using either GCN or GAT as the backbone, CANET consistently outperforms the corresponding competitors by a significant margin on the OOD data across two types of distribution shifts and three datasets, and yield highly competitive results on the ID data. This demonstrates the effectiveness of our proposed model for OOD generalization with a guarantee of decent performance on the ID data. Apart from the relative improvement over the competitors, we observed that on Cora and Citeseer, the absolute performance of CANET on the OOD data is very close to that on ID data. These results show that our model can effectively handle distribution shifts w.r.t. node features and graph structures.

Distribution Shifts on Temporal Graphs. In Table 3 we report the testing accuracy on Arxiv where we further divide the out-of-distribution data into three-fold according to the publication years of papers: we use papers published within 2014-2016 as OOD 1, 2016-2018 as OOD 2, and 2018-2020 as OOD 3. As the time gap between training and testing data goes large, the distribution shift becomes more significant as observed by [39], and we found that the performance of all the models exhibits a more or less degradation. In contrast with other models, however, the performance drop of CANET is much less severe, and our two model versions outperform the corresponding competitors by a large margin on the most difficult 2018-2020 testing set, with 14.1% and 27.4% improvements over the runner-up, respectively.

Distribution Shifts across Subgraphs. Table 3 also presents the testing ROC-AUC on Twitch where we compare the performance on three OOD subgraphs separately (here OOD 1/2/3 refers to the subgraph ES/FR/EN). This dataset is challenging for generalization, since the nodes in different subgraphs are disconnected and the model needs to generalize to nodes in new unseen graphs collected with different context (i.e., regions). We found CANET achieves overall superior performance over the competitors. This demonstrates the efficacy of our model for tackling OOD generalization across graphs in inductive learning.

Distribution Shifts across Dynamic Graph Snapshots. We report the macro F1 score of testing data on Elliptic in Fig. 4. Since the out-of-distribution data contains snapshots of a long time span, we chronologically split these testing snapshots into eight subsets with an equal size. Overall, we found that CANET can yield consistently better performance than other competitors, with average 12.16% improvement over the runner-ups. Notably, the performance gap between CANET and the runner-ups that differ in each subset is significantly larger than the margin among other competitors. These results can be strong evidence that verifies the

Table 1: Test (mean±standard deviation) Accuracy (%) for citation networks on out-of-distribution (OOD) and in-distribution (ID) data. OOM indicates out-of-memory error on a GPU with 16GB memory.

Backbone	Method	Cora		Citeseer		Pubmed	
		OOD	ID	OOD	ID	OOD	ID
GCN	ERM	74.30 ± 2.66	94.83 ± 0.25	74.93 ± 2.39	85.76 ± 0.26	81.36 ± 1.78	92.76 ± 0.10
	IRM	74.19 ± 2.60	94.88 ± 0.18	75.34 ± 1.61	85.34 ± 0.46	81.14 ± 1.72	92.80 ± 0.12
	Coral	74.26 ± 2.28	94.89 ± 0.18	74.97 ± 2.53	85.64 ± 0.28	81.56 ± 2.35	92.78 ± 0.11
	DANN	73.09 ± 3.24	95.03 ± 0.16	74.74 ± 2.78	85.75 ± 0.49	80.77 ± 1.43	93.20 ± 0.42
	GroupDRO	74.25 ± 2.61	94.87 ± 0.25	75.02 ± 2.05	85.33 ± 0.36	81.07 ± 1.89	92.76 ± 0.08
	Mixup	92.77 ± 1.27	94.84 ± 0.30	77.28 ± 5.28	85.00 ± 0.50	79.76 ± 4.44	92.68 ± 0.13
	SRGNN	81.91 ± 2.64	95.09 ± 0.32	76.10 ± 4.04	85.84 ± 0.37	84.75 ± 2.38	93.52 ± 0.31
	EERM	83.00 ± 0.77	89.17 ± 0.23	74.76 ± 1.15	83.81 ± 0.17	OOM	OOM
	CANET	96.12 ± 1.04	97.87 ± 0.23	94.57 ± 1.92	95.18 ± 0.17	88.82 ± 2.30	97.37 ± 0.11
GAT	ERM	91.10 ± 2.26	95.57 ± 0.40	82.60 ± 0.51	89.02 ± 0.32	84.80 ± 1.47	93.98 ± 0.24
	IRM	91.63 ± 1.27	95.72 ± 0.31	82.73 ± 0.37	89.11 ± 0.36	84.95 ± 1.06	93.89 ± 0.26
	Coral	91.82 ± 1.30	95.74 ± 0.39	82.44 ± 0.58	89.05 ± 0.37	85.07 ± 0.95	94.05 ± 0.23
	DANN	92.40 ± 2.05	95.66 ± 0.28	82.49 ± 0.67	89.02 ± 0.31	83.94 ± 0.84	93.46 ± 0.31
	GroupDRO	90.54 ± 0.94	95.38 ± 0.23	82.64 ± 0.61	89.13 ± 0.27	85.17 ± 0.86	94.00 ± 0.18
	Mixup	92.94 ± 1.21	94.66 ± 0.10	82.77 ± 0.30	89.05 ± 0.05	81.58 ± 0.65	92.79 ± 0.18
	SRGNN	91.77 ± 2.43	95.36 ± 0.24	82.72 ± 0.35	89.10 ± 0.15	83.40 ± 0.67	93.21 ± 0.29
	EERM	91.80 ± 0.73	91.37 ± 0.50	74.07 ± 0.75	83.53 ± 0.56	OOM	OOM
	CANET	97.30 ± 0.25	95.94 ± 0.29	95.33 ± 0.33	89.57 ± 0.65	89.89 ± 1.92	95.04 ± 0.16

Table 2: Statistics for experimental datasets.

Datasets	#Nodes	#Edges	#Classes	#Features	Shift Types
Cora	2708	5429	7	1433	spurious features
Citeseer	3327	4732	6	3703	spurious features
Pubmed	19717	44338	3	500	spurious features
Twitch	34120	892346	2	2545	disconnected subgraphs
Arxiv	169343	1166243	40	128	time attributes
Elliptic	203769	234355	2	165	dynamic snapshots

superiority of our model for generalizing to previously unseen graph snapshots in the future.

5.3 Ablation Studies (R2)

Ablation Study on Regularization Loss. We remove the regularization loss term in Eqn. 5 and only use the supervised loss for training. We compare the learning curves (training accuracy and testing accuracy on OOD-Struct) of our model and its simplified variant on Cora in Fig. 5(a). We found that the regularization loss can indeed help to improve generalization to OOD testing data. In Fig. 5(b), we further report the OOD testing accuracy on Arxiv after removing the regularization loss (*w/o Reg Loss*) and replacing the trivial prior distribution $p_0(E)$ with a complex one (*w/ VPrior Reg*), i.e., using the generated results from random inputs to estimate the probability as is done by [34]. The results again verify the effectiveness of the regularization loss for generalization, and further show that using trivial uniform distribution for $p_0(E)$ works better than the complex one since it can push the model to equally attend on each pseudo environment candidate as an effective regularization for facilitating generalization.

Ablation Study on Environment Inference. We further replace the pseudo environment representation $e_u^{(l)}$ for each layer by a single one e_u that is shared across all layers. In such a case, the model degrades to a simplified variant (called *w/o Layer Env* where the global pseudo environment estimation controls the propagation in each layer. Moreover, we further replace the trainable

environment estimator with a non-parametric mean pooling over K propagation branches at each layer (we call this variant *w/o Para Env*). Fig. 5(b) presents the results of these two simplified variants on Arxiv where we can see clear performance drop in both cases, which validates the effectiveness of the layer-dependent environment inference that can provide better capacity to capture complex structural patterns useful for generalization.

5.4 Hyper-parameter Analysis (R3)

Impact of K . We study the impact of the number of pseudo environments K and present the results in Fig. 6(a) and 6(b) where we increase K from 2 to 7 on Arxiv and Twitch, respectively. We found that the model performance on OOD data is overall not sensitive to the value of K on Twitch. On Arxiv, different K 's have negligible impact on the performance on the testing set OOD 1 and affect the performance on the other two testing sets to a certain degree. The possible reason is that the distribution shifts of the latter are more significant than the former and the generalization would be more challenging. In such cases, smaller K may not be expressive for learning informative pseudo environments and larger K may lead to potential redundancy and over-fitting.

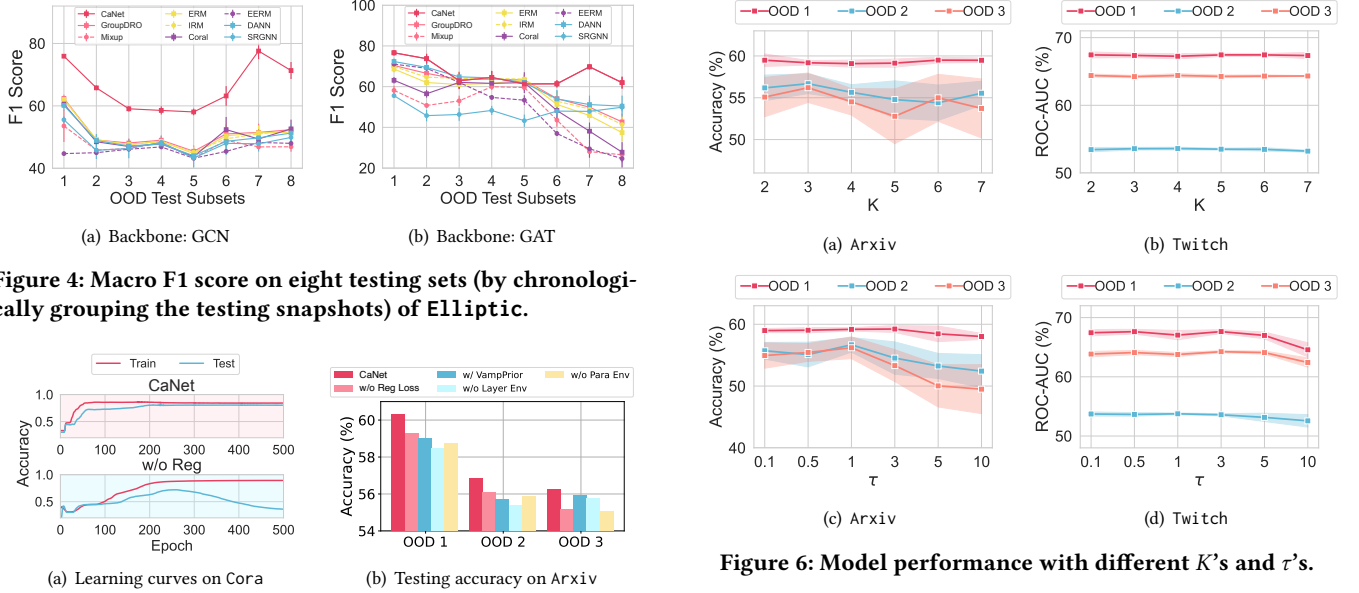
Impact of τ . We next investigate into the impact of the temperature coefficient τ in the Gumbel-Softmax. In Fig. 6(c) and 6(d) we present the performance on different OOD sets of Arxiv and Twitch, respectively, w.r.t. the variation of τ . We found that a moderate value of τ (e.g., $\tau = 1$) contributes to the best performance. Overall, smaller τ can yield stably good performance, while larger τ would cause performance drop. The reason could be that τ controls the sharpness of the sampled results, and excessively large τ tends to over-smooth the output, thereby causing samples to converge towards an uninformative uniform distribution.

5.5 Visualization (R4)

We visualize the weights $W_D^{(l,k)}$ of different branches ($K = 3$) at the first and the last layers on Arxiv and Twitch in Fig. 7, 8, 9 and

Table 3: Test (mean±standard deviation) Accuracy (%) for Arxiv and ROC-AUC (%) for Twitch on different subsets of out-of-distribution data. We use publication years and subgraphs for data splits on Arxiv and Twitch, respectively.

Backbone	Method	Arxiv				Twitch			
		OOD 1	OOD 2	OOD 3	ID	OOD 1	OOD 2	OOD 3	ID
GCN	ERM	56.33 ± 0.17	53.53 ± 0.44	45.83 ± 0.47	59.94 ± 0.45	66.07 ± 0.14	52.62 ± 0.01	63.15 ± 0.08	75.40 ± 0.01
	IRM	55.92 ± 0.24	53.25 ± 0.49	45.66 ± 0.83	60.28 ± 0.23	66.95 ± 0.27	52.53 ± 0.02	62.91 ± 0.08	74.88 ± 0.02
	Coral	56.42 ± 0.26	53.53 ± 0.54	45.92 ± 0.52	60.16 ± 0.12	66.15 ± 0.14	52.67 ± 0.02	63.18 ± 0.03	75.40 ± 0.01
	DANN	56.35 ± 0.11	53.81 ± 0.33	45.89 ± 0.37	60.22 ± 0.29	66.15 ± 0.13	52.66 ± 0.02	63.20 ± 0.06	75.40 ± 0.02
	GroupDRO	56.52 ± 0.27	53.40 ± 0.29	45.76 ± 0.59	60.35 ± 0.27	66.82 ± 0.26	52.69 ± 0.02	62.95 ± 0.11	75.03 ± 0.01
	Mixup	56.67 ± 0.46	54.02 ± 0.51	46.09 ± 0.58	60.09 ± 0.15	65.76 ± 0.30	52.78 ± 0.04	63.15 ± 0.08	75.47 ± 0.06
	SRGNN	56.79 ± 1.35	54.33 ± 1.78	46.24 ± 1.90	60.02 ± 0.52	65.83 ± 0.45	52.47 ± 0.06	62.74 ± 0.23	75.75 ± 0.09
	EERM	OOM	OOM	OOM	OOM	67.50 ± 0.74	51.88 ± 0.07	62.56 ± 0.02	74.85 ± 0.05
	CaNet	59.01 ± 0.30	56.88 ± 0.70	56.27 ± 1.21	61.42 ± 0.10	67.47 ± 0.32	53.59 ± 0.19	64.24 ± 0.18	75.10 ± 0.08
GAT	ERM	57.15 ± 0.25	55.07 ± 0.58	46.22 ± 0.82	59.72 ± 0.35	65.67 ± 0.02	52.00 ± 0.10	61.85 ± 0.05	75.75 ± 0.15
	IRM	56.55 ± 0.18	54.53 ± 0.32	46.01 ± 0.33	59.94 ± 0.18	67.27 ± 0.19	52.85 ± 0.15	62.40 ± 0.24	75.30 ± 0.09
	Coral	57.40 ± 0.51	55.14 ± 0.71	46.71 ± 0.61	60.59 ± 0.30	67.12 ± 0.03	52.61 ± 0.01	63.41 ± 0.01	75.20 ± 0.01
	DANN	57.23 ± 0.18	55.13 ± 0.46	46.61 ± 0.57	59.72 ± 0.14	66.59 ± 0.38	52.88 ± 0.12	62.47 ± 0.32	75.82 ± 0.27
	GroupDRO	56.69 ± 0.27	54.51 ± 0.49	46.00 ± 0.59	60.03 ± 0.32	67.41 ± 0.04	52.99 ± 0.08	62.29 ± 0.03	75.74 ± 0.02
	Mixup	57.17 ± 0.33	55.33 ± 0.37	47.17 ± 0.84	59.84 ± 0.50	65.58 ± 0.13	52.04 ± 0.04	61.75 ± 0.13	75.72 ± 0.07
	SRGNN	56.69 ± 0.38	55.01 ± 0.55	46.88 ± 0.58	59.39 ± 0.17	66.17 ± 0.03	52.84 ± 0.04	62.07 ± 0.04	75.45 ± 0.03
	EERM	OOM	OOM	OOM	OOM	66.80 ± 0.46	52.39 ± 0.20	62.07 ± 0.68	75.19 ± 0.50
	CaNet	60.44 ± 0.27	58.54 ± 0.72	59.61 ± 0.28	62.91 ± 0.35	68.08 ± 0.19	53.49 ± 0.14	63.76 ± 0.17	76.14 ± 0.07

**Figure 4: Macro F1 score on eight testing sets (by chronologically grouping the testing snapshots) of Elliptic.****Figure 5: Ablation studies. (a) Learning curves on Cora w/ and w/o regularization loss. (b) Ablation results on Arxiv.**

10 (located in the appendix), respectively. We found the weights of different branches exhibit clear differences, which suggests that the K branches in the MoE architecture transform node embeddings in different manners and indeed learn distinct patterns from observed data. In fact, each branch corresponds to one pseudo environment, and this gives rise to an expressive model that helps to exploit predictive relations useful for generalization.

6 CONCLUSION

In this paper, we focus on the generalization of graph neural networks w.r.t. node-level distribution shifts which require the model

Figure 6: Model performance with different K 's and τ 's.

to deal with out-of-distribution nodes from testing set. Our methodology is built on causal analysis for the learning behaviors of GNNs trained with MLE loss on observed data, on top of which we propose a new learning objective that is provably effective for capturing environment-insensitive predictive relations between ego-graph features and node labels. Extensive empirical results verify the effectiveness of the proposed model for handling various distribution shifts in graph-based node property prediction.

Future Works. There exist some interesting aspects that can be explored in future works. One promising direction is to extend the model architecture from standard graph neural networks (that focus on local message passing) to graph Transformers (that consider global attention) [40, 41]. Another potential direction is to apply the methodology to handle out-of-distribution generalization in domain-specific applications, like molecular discovery [43].

REFERENCES

- [1] Martin Arjovsky, Léon Bottou, Ishaan Gulrajani, and David Lopez-Paz. 2019. Invariant risk minimization. *arXiv preprint arXiv:1907.02893* (2019).
- [2] Gleb Bazhenov, Denis Kuznedelev, Andrey Malinin, Artem Babenko, and Liudmila Prokhorenkova. 2023. Evaluating Robustness and Uncertainty of Graph Models Under Structural Distributional Shifts. *arXiv preprint arXiv:2302.13875* (2023).
- [3] Beatrice Bevilacqua, Yangze Zhou, and Bruno Ribeiro. 2021. Size-Invariant Graph Representations for Graph Classification Extrapolations. In *International Conference on Machine Learning (ICML)*. 837–851.
- [4] Davide Buffelli, Pietro Lió, and Fabio Vandin. 2022. SizeShiftReg: a Regularization Method for Improving Size-Generalization in Graph Neural Networks. In *NeurIPS*.
- [5] Peter Bühlmann. 2018. Invariance, causality and robustness. *CoRR abs/1812.08233* (2018).
- [6] Ming Chen, Zhewei Wei, Zengfeng Huang, Bolin Ding, and Yaliang Li. 2020. Simple and Deep Graph Convolutional Networks. In *ICML*. 1725–1735.
- [7] Shaohua Fan, Xiao Wang, Chuan Shi, Peng Cui, and Bai Wang. 2021. Generalizing Graph Neural Networks on Out-Of-Distribution Graphs. *arXiv preprint arXiv:2111.10657* (2021).
- [8] Yaroslav Ganin, Evgeniya Ustinova, Hana Ajakan, Pascal Germain, Hugo Larochelle, François Laviolette, Mario Marchand, and Victor S. Lempitsky. 2016. Domain-Adversarial Training of Neural Networks. *J. Mach. Learn. Res.* 17 (2016), 59:1–59:35.
- [9] Mingming Gong, Kun Zhang, Tongliang Liu, Dacheng Tao, Clark Glymour, and Bernhard Schölkopf. 2016. Domain Adaptation with Conditional Transferable Components. In *International Conference on Machine Learning (ICML)*. 2839–2848.
- [10] Marco Gori, Gabriele Monfardini, and Franco Scarselli. 2005. A new model for learning in graph domains. *IEEE Trans. Neural Networks* 2, 1 (2005), 729–734.
- [11] Shengnan Guo, Youfang Lin, Ning Feng, Chao Song, and Huaiyu Wan. 2019. Attention Based Spatial-Temporal Graph Convolutional Networks for Traffic Flow Forecasting. In *AAAI*. 922–929.
- [12] William L. Hamilton, Zhitaoying, and Jure Leskovec. 2017. Inductive Representation Learning on Large Graphs. In *NeurIPS*. 1024–1034.
- [13] Weihua Hu, Matthias Fey, Marinka Zitnik, Yuxiao Dong, Hongyu Ren, Bowen Liu, Michele Catasta, and Jure Leskovec. 2020. Open Graph Benchmark: Datasets for Machine Learning on Graphs. In *NeurIPS 2020*, Hugo Larochelle, Marc'Aurelio Ranzato, Raia Hadsell, Maria-Florina Balcan, and Hsuan-Tien Lin (Eds.).
- [14] Thomas N. Kipf and Max Welling. 2017. Semi-Supervised Classification with Graph Convolutional Networks. In *ICLR*.
- [15] Johannes Klicpera, Aleksandar Bojchevski, and Stephan Günnemann. 2019. Pre-dict then Propagate: Graph Neural Networks meet Personalized PageRank. In *ICLR*.
- [16] Pang Wei Koh, Shiori Sagawa, Henrik Marklund, Sang Michael Xie, Marvin Zhang, Akshay Balsubramani, Weihua Hu, Michihiro Yasunaga, Richard Lanus Phillips, Irena Gao, Tony Lee, Etienne David, Ian Stavness, Wei Guo, Berton Earnshaw, Imran Haque, Sara M. Beery, Jure Leskovec, Anshul Kundaje, Emma Pierson, Sergey Levine, Chelsea Finn, and Percy Liang. 2021. WILDS: A Benchmark of in-the-Wild Distribution Shifts. In *International Conference on Machine Learning (ICML)*. 5637–5664.
- [17] David Krueger, Ethan Caballero, Joern-Henrik Jacobsen, Amy Zhang, Jonathan Binas, Dinghui Zhang, Remi Le Priol, and Aaron Courville. 2021. Out-of-distribution generalization via risk extrapolation (rex). In *ICML*.
- [18] Haoyang Li, Xin Wang, Ziwei Zhang, and Wenwu Zhu. 2022. Ood-gnn: Out-of-distribution generalized graph neural network. *TKDE* (2022).
- [19] Zenan Li, Qitian Wu, Fan Nie, and Junchi Yan. 2022. GraphDE: A Generative Framework for Debaised Learning and Out-of-Distribution Detection on Graphs. In *Advances in Neural Information Processing Systems*.
- [20] Shikun Liu, Tianchun Li, Yongbin Feng, Nhan Tran, Han Zhao, Qiang Qiu, and Pan Li. 2023. Structural Re-weighting Improves Graph Domain Adaptation. In *International Conference on Machine Learning*.
- [21] Yang Liu, Xiang Ao, Fuli Feng, Yunshan Ma, Kuan Li, Tat-Seng Chua, and Qing He. 2023. FLOOD: A Flexible Invariant Learning Framework for Out-of-Distribution Generalization on Graphs. In *ACM SIGKDD Conference on Knowledge Discovery and Data Mining*. 1548–1558.
- [22] Jiaqi Ma, Junwei Deng, and Qiaozhu Mei. 2021. Subgroup generalization and fairness of graph neural networks. *Advances in Neural Information Processing Systems* 34 (2021), 1048–1061.
- [23] Chris J. Maddison, Andriy Mnih, and Yee Whye Teh. 2017. The Concrete Distribution: A Continuous Relaxation of Discrete Random Variables. In *ICLR*.
- [24] Aldo Pareja, Giacomo Domeniconi, Jie Chen, Tengfei Ma, Toyotaro Suzumura, Hiroki Kanezashi, Tim Kaler, Tao B. Schardl, and Charles E. Leiserson. 2020. EvolveGCN: Evolving Graph Convolutional Networks for Dynamic Graphs. In *AAAI Conference on Artificial Intelligence (AAAI)*. 5363–5370.
- [25] Judea Pearl, Madelyn Glymour, and Nicholas P Jewell. 2016. Causal inference in statistics: A primer. *John Wiley & Sons* (2016).
- [26] Mateo Rojas-Carulla, Bernhard Schölkopf, Richard E. Turner, and Jonas Peters. 2018. Invariant Models for Causal Transfer Learning. *Journal of Machine Learning Research* 19 (2018), 36:1–36:34.
- [27] Benedek Rozemberczki and Rik Sarkar. 2021. Twitch Gamers: a Dataset for Evaluating Proximity Preserving and Structural Role-based Node Embeddings. *arXiv:2101.03091 [cs.SI]*
- [28] Shiori Sagawa, Pang Wei Koh, Tatsunori B Hashimoto, and Percy Liang. 2019. Distributionally robust neural networks for group shifts: On the importance of regularization for worst-case generalization. *arXiv preprint arXiv:1911.08731* (2019).
- [29] Franco Scarselli, Marco Gori, Ah Chung Tsoi, Markus Hagenbuchner, and Gabriele Monfardini. 2009. The Graph Neural Network Model. *IEEE Trans. Neural Networks* 20, 1 (2009), 61–80.
- [30] Prithviraj Sen, Galileo Namata, Mustafa Bilgic, Lise Getoor, Brian Galligher, and Tina Eliassi-Rad. 2008. Collective classification in network data. *AI magazine* 29, 3 (2008), 93–93.
- [31] Yongduo Sui, Qitian Wu, Jiancan Wu, Qing Cui, Longfei Li, Jun Zhou, Xiang Wang, and Xiangnan He. 2024. Unleashing the power of graph data augmentation on covariate distribution shift. *Advances in Neural Information Processing Systems* 36 (2024).
- [32] Baochen Sun and Kate Saenko. 2016. Deep coral: Correlation alignment for deep domain adaptation. In *Computer Vision—ECCV 2016 Workshops*. 443–450.
- [33] Jie Tang, Jimeng Sun, Chi Wang, and Zi Yang. 2009. Social influence analysis in large-scale networks. In *KDD. ACM*, 807–816.
- [34] Jakub Tomczak and Max Welling. 2018. VAE with a VampPrior. In *AISTATS*.
- [35] Petar Velickovic, Guillem Cucurull, Arantxa Casanova, Adriana Romero, Pietro Lió, and Yoshua Bengio. 2018. Graph Attention Networks. In *ICLR*.
- [36] Felix Wu, Amauri H. Souza Jr., Tianyi Zhang, Christopher Fifty, Tao Yu, and Kilian Q. Weinberger. 2019. Simplifying Graph Convolutional Networks. In *ICML, Kamalika Chaudhuri and Ruslan Salakhutdinov (Eds.)*. 6861–6871.
- [37] Qitian Wu, Yiting Chen, Chenxiao Yang, and Junchi Yan. 2023. Energy-based Out-of-Distribution Detection for Graph Neural Networks. In *International Conference on Learning Representations*.
- [38] Qitian Wu, Hengrui Zhang, Xiaofeng Gao, Peng He, Paul Weng, Han Gao, and Guihai Chen. 2019. Dual Graph Attention Networks for Deep Latent Representation of Multifaceted Social Effects in Recommender Systems. In *The World Wide Web Conference*. 2091–2102.
- [39] Qitian Wu, Hengrui Zhang, Junchi Yan, and David Wipf. 2022. Handling Distribution Shifts on Graphs: An Invariance Perspective. In *International Conference on Learning Representations*.
- [40] Qitian Wu, Wentao Zhao, Zenan Li, David P. Wipf, and Junchi Yan. 2022. NodeFormer: A Scalable Graph Structure Learning Transformer for Node Classification. In *Advances in Neural Information Processing Systems*.
- [41] Qitian Wu, Wentao Zhao, Chenxiao Yang, Hengrui Zhang, Fan Nie, Haitian Jiang, Yatao Bian, and Junchi Yan. 2023. SGFormer: Simplifying and Empowering Transformers for Large-Graph Representations. In *Advances in Neural Information Processing Systems (NeurIPS)*.
- [42] Chenxiao Yang, Qitian Wu, Jiahua Wang, and Junchi Yan. 2023. Graph Neural Networks are Inherently Good Generalizers: Insights by Bridging GNNs and MLPs. In *International Conference on Learning Representations*.
- [43] Nianzu Yang, Kaipeng Zeng, Qitian Wu, Xiaosong Jia, and Junchi Yan. 2022. Learning Substructure Invariance for Out-of-Distribution Molecular Representations. In *Advances in Neural Information Processing Systems*.
- [44] Nianzu Yang, Kaipeng Zeng, Qitian Wu, and Junchi Yan. 2023. MoleRec: Combinatorial Drug Recommendation with Substructure-Aware Molecular Representation Learning. In *The Web Conference*. 4075–4085.
- [45] Gilad Yehudai, Ethan Fetaya, Eli A. Meir, Gal Chechik, and Haggai Maron. 2021. From Local Structures to Size Generalization in Graph Neural Networks. In *International Conference on Machine Learning (ICML)*. 11975–11986.
- [46] Minji Yoon, Bryan Hooi, Kijung Shin, and Christos Faloutsos. 2019. Fast and Accurate Anomaly Detection in Dynamic Graphs with a Two-Pronged Approach. In *ACM SIGKDD International Conference on Knowledge Discovery*. 647–657.
- [47] Junchi Yu, Jian Liang, and Ran He. 2023. Mind the Label Shift of Augmentation-based Graph OOD Generalization. In *IEEE/CVF Conference on Computer Vision and Pattern Recognition*.
- [48] Hongyi Zhang, Moustapha Cisse, Yann N Dauphin, and David Lopez-Paz. 2017. mixup: Beyond empirical risk minimization. *arXiv preprint arXiv:1710.09412* (2017).
- [49] Tianqi Zhang, Qitian Wu, and Junchi Yan. 2023. Learning High-Order Graph Convolutional Networks via Adaptive Layerwise Aggregation Combination. *IEEE Trans. Neural Networks Learn. Syst.* 34, 8 (2023), 5144–5155.
- [50] Qi Zhu, Natalia Ponomareva, Jiawei Han, and Bryan Perozzi. 2021. Shift-robust gnn: Overcoming the limitations of localized graph training data. *NeurIPS* (2021), 27965–27977.
- [51] Marinka Zitnik and Jure Leskovec. 2017. Predicting multicellular function through multi-layer tissue networks. *Bioinform.* 33, 14 (2017), i190–i198. <https://doi.org/10.1093/bioinformatics/btx252>

A PROOFS AND DERIVATIONS

A.1 Derivation for Equation 4

We are to derive a tractable objective form for $\log p_\theta(\hat{Y}|do(G))$. Before the proof, we first introduce two fundamental rules of *do*-calculus [25] which will be used as the building blocks later. Consider a causal directed acyclic graph \mathcal{A} with three nodes: B , D and E . We denote $\mathcal{A}_{\overline{B}}$ as the intervened causal graph by cutting off all arrows coming into B , and \mathcal{A}_B as the graph by cutting off all arrows going out from B . For any interventional distribution compatible with \mathcal{A} , the *do*-calculus induces the following two fundamental rules.

i) Action/observation exchange:

$$P(d|do(b), do(e)) = P(d|do(b), e), \text{ if } (D \perp\!\!\!\perp E|B)_{\mathcal{A}_{\overline{BE}}}.$$

ii) Insertion/deletion of actions:

$$P(d|do(b), do(e)) = P(d|do(b)), \text{ if } (D \perp\!\!\!\perp E|B)_{\mathcal{A}_{\overline{BE}}}.$$

Back to our case where we have a causal graph with three variables E , G , \hat{Y} whose dependence relationships are shown in Fig. 2(b). We have

$$\begin{aligned} P(\hat{Y}|do(G)) &= \sum_e P(\hat{Y}|do(G), E=e)P(E=e|do(G)) \\ &= \sum_e P(\hat{Y}|G, E=e)P(E=e|do(G)) \\ &= \sum_e P(\hat{Y}|G, E=e)P(E=e), \end{aligned} \quad (12)$$

where the first step is given by the law of total probability, the second step is according to the first rule (since $\hat{Y} \perp\!\!\!\perp G|E$ in $\mathcal{A}_{\overline{G}}$), and the third step is due to the second rule (since we have $E \perp\!\!\!\perp G$ in $\mathcal{A}_{\overline{G}}$). The above derivation shows that

$$p_\theta(\hat{Y}|do(G)) = \mathbb{E}_{p_0(E)} [p_\theta(\hat{Y}|G, E)], \quad (13)$$

where p_0 is the prior distribution of environments.

A.2 Derivation for Equation 5

We derive a variational lower bound for $\log p_\theta(\hat{Y}|do(G))$:

$$\begin{aligned} &\log \sum_e p_\theta(\hat{Y}|G, E=e)P(E=e) \\ &= \log \sum_e p_\theta(\hat{Y}|G, E=e)p_0(E=e) \frac{q_\phi(E=e|G)}{q_\phi(E=e|G)} \\ &\geq \sum_e q_\phi(E=e|G) \log p_\theta(\hat{Y}|G, E=e)p_0(E=e) \frac{1}{q_\phi(E=e|G)} \\ &= \sum_e q_\phi(E=e|G) \log p_\theta(\hat{Y}|G, E=e) \\ &\quad - \sum_e q_\phi(E=e|G) \log \frac{q_\phi(E=e|G)}{p_0(E=e)}, \end{aligned} \quad (14)$$

where the penultimate step uses the Jensen's Inequality. The above derivation gives rise to

$$\begin{aligned} &\log p_\theta(\hat{Y}|do(G)) \\ &\geq \mathbb{E}_{q_\phi(E|G)} [\log p_\theta(\hat{Y}|G, E)] - KL(q_\phi(E|G) \| p_0(E)). \end{aligned} \quad (15)$$

Algorithm 1 Feed-forward and Training for CANET.

- 1: **Input:** Input node features $\mathbf{X} = [\mathbf{x}_v]_{v \in \mathcal{V}}$, adjacency matrix \mathbf{A} . Initialized GNN predictor parameter θ , initialized environment estimator parameter ϕ . α_1 , learning rate for ϕ . α_2 , learning rate for θ . $\beta_1 = 0.9$, $\beta_2 = 0.999$, Adam parameters.
- 2: **while** not converged **do**
- 3: Compute initial node embeddings $\mathbf{z}_v^{(1)} = \phi_{in}(\mathbf{x}_v)$;
- 4: **for** $l = 1$ **to** L **do**
- 5: Estimate pseudo environment distribution $\pi_v^{(l)}$ via (6) for $v \in \mathcal{V}$;
- 6: Obtain inferred pseudo environment $\mathbf{e}_v^{(l)}$ through (7) for $v \in \mathcal{V}$;
- 7: **if** use the propagation of CANET-GCN **then**
- 8: Update node embeddings $\mathbf{z}_v^{(l+1)}$ with (8);
- 9: **end if**
- 10: **if** use the propagation of CANET-GAT **then**
- 11: Update node embeddings $\mathbf{z}_v^{(l+1)}$ with (9);
- 12: **end if**
- 13: **end for**
- 14: Compute predicted labels $\hat{\mathbf{y}}_v = \phi_{out}(\mathbf{z}_v^{(L+1)})$;
- 15: Compute loss \mathcal{L} based on (11);
- 16: Update the environment estimator $\phi \leftarrow \text{Adam}(\mathcal{L}, \phi, \alpha_1, \beta_1, \beta_2)$
- 17: Update the GNN predictor $\theta \leftarrow \text{Adam}(\mathcal{L}, \theta, \alpha_2, \beta_1, \beta_2)$
- 18: **end while**
- 19: **Output:** Trained model parameters θ^* , ϕ^* .

B DATASET INFORMATION

◦ Cora, Citeseer and Pubmed are three commonly used citation networks [30] for node property prediction. Since there is no explicit information that can be used to partition the nodes from distinct distributions, we consider a synthetic way that creates spurious node features for introducing distribution shifts. Specifically, for each dataset, we keep the original node labels in the dataset and synthetically create node features to generate graphs from multiple domains (with id $i = 1, 2, 3, 4, 5, 6$) that involve distribution shifts. For creating domain-specific node features, we consider a randomly initialized GCN network: it takes the node label \mathbf{y}_v and domain id i to generate spurious node features $\tilde{\mathbf{x}}_v^{(i)}$ for the i -th domain. Then we concatenate the generated features with the original one $\mathbf{x}_v^{(i)} = [\mathbf{x}_v \| \tilde{\mathbf{x}}_v^{(i)}]$ as the node features $\mathbf{X}^{(i)} = [\mathbf{x}_v^{(i)}]_{v \in \mathcal{V}}$ of the i -th domain. Then we use the graphs with node features $\mathbf{X}^{(1)}$, $\mathbf{X}^{(2)}$ and $\mathbf{X}^{(3)}$ as ID data. The OOD data consists of three graphs with node features $\mathbf{X}^{(4)}$, $\mathbf{X}^{(5)}$ and $\mathbf{X}^{(6)}$, respectively. These synthetic datasets can be used for testing the model when generalizing to OOD data with distribution shifts of node features.

◦ Twitch is a multi-graph dataset [27] where each subgraph is a social network from a particular region. We use the nodes in different subgraphs for data splitting, since these subgraphs have different sizes, densities and node degrees [39]. In specific, we use the nodes from subgraphs DE, PT, RU as in-distribution data and the nodes from subgraphs ES, FR, EN as out-of-distribution data.

◦ Arxiv is a temporal citation network [13] where each node, a paper, has a time label indicating the publication year. The papers published in different years can be seen as samples from different distributions, and the distribution shift becomes more significant when the time gap between training and testing is enlarged. We use the papers published between 2005 and 2014 as in-distribution data, and the papers published after 2014 as out-of-distribution data.

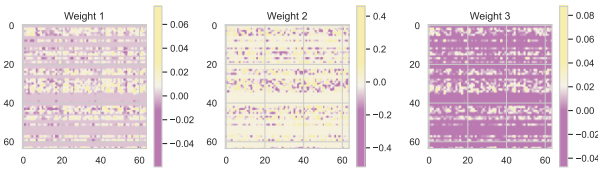


Figure 7: Visualization of the model weights of different branches ($K = 3$) at the first layer on Arxiv.

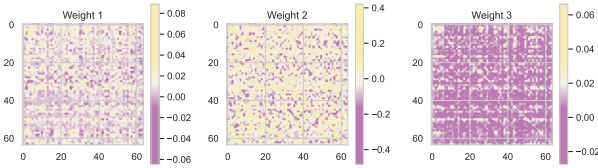


Figure 8: Visualization of the model weights of different branches ($K = 3$) at the last layer on Arxiv.

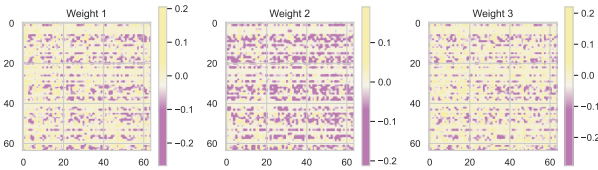


Figure 9: Visualization of the model weights of different branches ($K = 3$) at the first layer on Twitch.

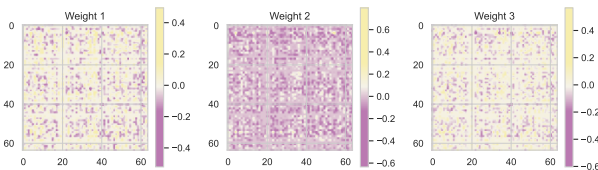


Figure 10: Visualization of the model weights of different branches ($K = 3$) at the last layer on Twitch.

◦ Elliptic is a dynamic graph for bitcoin transaction records [24] that comprise a sequence of graph snapshots where each snapshot is generated at one time. We can naturally treat nodes in different snapshots as samples from different distributions since the underlying mechanism behind transactions is heavily dependent on the time and market. We use the first five graph snapshots as in-distribution data and the remaining snapshots as out-of-distribution data.

C IMPLEMENTATION DETAILS

Our implementation is based on PyTorch 1.13.0 and PyTorch Geometric 2.1.0. All of our experiments are run on a Tesla V100 with 16 GB memory. We adopt Adam with weight decay for training and set a fixed training budget with 500 epochs. The testing performance achieved by the epoch where the model gives the best performance on validation data is reported.

C.1 Hyper-parameter Settings

We instantiate ϕ_{in} and ϕ_{out} as a fully-connected layer. The detailed architecture of CANET is described as follows. The model architecture consists of the following modules in sequential order:

- A fully-connected layer with hidden size $D \times H$ (transforming D -dim input raw features into H -dim embeddings).
- L -layer GNN network with hidden size $H \times H$ (each layer contains K branches that have independent parameterization), based on the two instantiations in Sec. 4.3.
- A fully-connected layer with hidden size $H \times C$ (mapping H -dim embeddings to C classes).

In each layer, we use ReLU activation, dropout and residual link. For model hyper-parameters, we search them for each dataset with grid search on the validation set. The searching spaces for all the hyper-parameters are as follows.

- Number of GNN layers L : [2,3,4,5].
- Hidden dimension H : [32, 64, 128].
- Dropout ratio: [0.0, 0.1, 0.2, 0.5].
- Learning rate: [0.001, 0.005, 0.01, 0.02].
- Weight decay: [0, 5e-5, 5e-4, 5e-3].
- Number of pseudo environments K : [3,5,10].
- Gumbel-Softmax temperature τ : [1, 3, 5, 10].

C.2 Competitors

For competitors, we use their public implementation. We also use the validation set to tune the hyper-parameters (GNN layers, hidden dimension, dropout ratio and learning rate) using the same searching space as ours. For other hyper-parameters that differ in each model, we refer to their default settings reported by the original paper. We present more information for these competitors below.

The first line of competitors is designed for handling out-of-distribution generalization in the general setting, e.g., image data, where the samples are assumed to be independent. The competitors include IRM [1], DeepCoral [32], DANN [8], GroupDRO [28] and Mixup [48]. These approaches resort to different strategies to improve the generalization of the model. Mixup aims to augment the training data by interpolation of the observed samples, while other four methods propose robust learning algorithms that can guide the model to learn stable predictive relations against distribution shifts. For accommodating the structural information and data interdependence, We use GCN and GAT as the encoder backbone for computing node representation and predicting node labels.

Another line of works concentrates on out-of-distribution generalization with graph data, where the observed samples (i.e., nodes) are inter-connected, including two recently proposed models SR-GNN [50] and EERM [39]. SR-GNN proposes a regularization loss for enhancing the generalization of the model to new data. EERM leverages the invariance principle to develop an adversarial training approach for environment exploration. These models are agnostic to encoder backbones. For fair comparison, we use GCN and GAT as their encoder backbones.